

Numerical modelling of magnetic nanoparticle behavior in an alternating magnetic field based on multiphysics coupling

A. Ashofteh, R. Marqués, A. Callejas, R. Muñoz & J. Melchor

To cite this article: A. Ashofteh, R. Marqués, A. Callejas, R. Muñoz & J. Melchor (2022): Numerical modelling of magnetic nanoparticle behavior in an alternating magnetic field based on multiphysics coupling, *Mechanics of Advanced Materials and Structures*, DOI: [10.1080/15376494.2022.2136805](https://doi.org/10.1080/15376494.2022.2136805)

To link to this article: <https://doi.org/10.1080/15376494.2022.2136805>



Published online: 21 Nov 2022.



Submit your article to this journal [↗](#)








View related articles [↗](#)



View Crossmark data [↗](#)

Numerical modelling of magnetic nanoparticle behavior in an alternating magnetic field based on multiphysics coupling

A. Ashofteh^{a,b,c} , R. Marqués^a , A. Callejas^{c,d} , R. Muñoz^e , and J. Melchor^{a,b,c} 

^aDepartment of Statistics and Operations Research, University of Granada, Granada, Spain; ^bMNat Scientific Unit of Excellence, University of Granada, Spain; ^cInstituto de Investigación Biosanitaria, ibs.GRANADA, Spain; ^dDepartment of Structural Mechanics, University of Granada, Granada, Spain; ^eDepartment of Civil Engineering, University of Granada, Granada, Spain

ABSTRACT

In magnetic nanoparticle hyperthermia, the magnetic nanoparticles (MNPs) start oscillations when they are exposed to an alternating magnetic field, which may generate ultrasound waves. These resulting oscillations of nanoparticles can lead to the movement of drug carrier liposomes. In this study, a multiphysics coupling model of magnetic nanoparticle behavior in an alternating magnetic field was developed, implementing solid mechanics compliance parameters and piezomagnetic coupling matrices. A detailed sensitivity study was conducted to examine the effects of size and elastic modulus of MNPs, distribution and distance between two MNPs, elasticity and viscosity of the glycerol medium and mesh element sizes on the output displacement signals of MNPs. The results indicated that magnetic nanoparticles undergo some displacements when they are exposed to an alternating magnetic field. These oscillations may generate ultrasound waves, though the amount of displacement for each nanoparticle is negligibly small. It is expected that aggregated nanoparticles result in much higher oscillations.

ARTICLE HISTORY

Received 15 June 2022
Accepted 12 October 2022

KEYWORDS

Magnetic nanoparticle hyperthermia; alternating magnetic field; drug delivery; multiphysics

1. Introduction

Magnetic hyperthermia is based on the use of magnetic nanoparticles (MNPs) to increase the temperature at the MNP-loaded target tissue. The procedure involves the dispersion of MNPs throughout the target tissue, while the MNPs absorb energy from the magnetic field and dissipate it in terms of heat to the target tissue [1]. Power absorption by MNPs under an alternating magnetic field is the source of heating properties used for magnetic hyperthermia. The basic mechanisms for power absorption are related with the relaxation of the magnetic moments within single-domain nanoparticles. The relaxation can occur by Neel relaxation between the hard and easy magnetization axes of the magnetic material and by physical rotation of the MNPs, if they are immersed in a carrier liquid (Brown relaxation) [2, 3].

In the recent years, many experimental and numerical researches have been done in the field of magnetic nanoparticle hyperthermia. Some studies have demonstrated cancer cell death due to the increased temperature at the target tissue [4, 5], while there are some more studies which have demonstrated the possibility of cell death without increasing the temperature [2, 6, 7]. It is believed that additional mechanisms are involved in triggering cell death. When magnetic nanoparticles are exposed to the alternating magnetic field, they start oscillations which can generate ultrasound waves [8]. This effect could permit to generate ultrasound in cells which have internalized magnetic nanoparticles (MNPs). The induced

ultrasound may be effective in killing the cancer cells of a tumor [8]. These resulting oscillations of nanoparticles may lead to the movement of drug carrier liposomes, which can be very useful for an efficient targeting in drug delivery. This approach could be used in combination with all conventional treatments, e.g., chemo- and radiotherapy [9]. The potential outcome of this hypothesis could include novel sensing and therapeutic strategies like mechanical intracellular actuation, new imaging protocols, and selective biomolecular detection.

Theoretically, the effect of ultrasound generation is maximized a static magnetic field is superimposed on an alternating one. Carrey et al. proposed for the first time, that superposition of an alternating and a static magnetic field is a promising way to result in a generation of ultrasound of 100KHz of frequency in this case. This effect could generate ultrasound stimulation in cells, which may support a efficient targeting in drug delivery and therapy with the same level of energy (Eq. 1) [8]. The next equation describes the relationship between magnetic maximum gradient, mechanical velocity and peak-to-peak amplitude of the oscillation for a single nanoparticle in an in vitro set up:

$$\begin{cases} v_{stat} = \frac{VM\nabla B_{max}}{6\pi\eta R} \\ d = \frac{v_{stat}}{4f} \end{cases} \quad (1)$$

where v_{stat} is stationary velocity [m/s], V is the volume of nanoparticle [m^3], M is the nanoparticle magnetization [A/

m] (A , ampere), ∇B is the magnetic gradient [T/m] (T , tesla), η is the viscosity of medium [$Pa \cdot s$], R is the radius of nanoparticle [m], d is the peak to peak amplitude of the displacement [m] and f is the applied frequency [kHz].

Numerous studies focused on the numerical methods for the optimization of treatment parameters. A first group of them solves the magneto-thermal field separately, offering useful conclusions. [10–15]. Candeo et al. [11] developed a numerical finite element magnetic fluid hyperthermia model of abdomen district using anatomical CT images. He concluded that the main parameters to critically influence the heating effects are; radius and volume concentration of MNPs, the frequency and magnitude of the applied magnetic field. Wu et al. [16] employed the power density obtained from electromagnetic field simulation as a heat source into Penne's bio-heat transfer equation. His results indicated that the magnetic field generated by the Helmholtz coil can effectively heat target tissues without collateral tissue damage. However, there are not enough modellizations that incorporates the magnetic and thermal fields together in a single calculation to monitor the heating distribution in tumors. For example, Li et al. developed a multiphysics coupling model of magnetic fluid hyperthermia to solve the magnetic losses of magnetic nanoparticles [17]. They proposed to adopt a higher range of field amplitude, nanoparticle radius and volume fraction at a lower frequency to provide a therapeutic effect for deep tumors.

In magnetic nanoparticle hyperthermia the maximum damage to the tumor must be insured, while protecting the normal tissue. Hence, an optimized algorithm is needed to determine the induced heating patterns. Salloum et al. developed the optimization algorithm to determine the optimum parameters of the heat sources for nanoparticle injection site [10, 18]. Moreover, parameters relating to the nanoparticle concentration, injection amount and rate should be also optimized.

The search for more effective and reliable nanomaterials is one of the main goals in biomedicine. Therapeutic applications rely on such nanosystems (e.g., nanoparticles) to achieve localized drug release, therefore decreasing the systemic toxicity that many therapeutic drugs have on patients [19]. An advantage is that, if properly designed, these nanosystems can be remotely triggered for drug release, providing spatial and temporal control of the administered doses. A major part of these efforts is based on electromagnetic and ultrasonic waves as the external stimuli to actuate the nanosystems, where the study of the magneto-mechanical coupling is more relevant than the magneto-thermal one. Magnetic nanoparticles (MNPs) and liposomes are the archetypes of nanosystems triggered by electromagnetic and ultrasonic waves, respectively. Indeed, for numerous types of medical diagnosis the safest, fastest and least expensive methods for scanning are the magnetic resonance imaging (MRI) using radiofrequency, and echography based on ultrasound (US). Both techniques sometimes require the use of contrast agents to improve image quality, and therefore the clinical market has already approved different types of MNP-based colloids (EndoremR, NanoThermR) [20] and liposomes (SonoVueR; SonaZoidR) [21] for this purpose.

On the other hand, the clinically available materials are known to be still sub-optimal regarding their efficiency and responsiveness to external waves and, accordingly, basic research on these nanosystems is presently oriented to establish the actual limits for their performance.

Liposomes have been used for delivering therapeutic and diagnostic agents to tumors [22], and there are currently different types available, some passive, some others designed for ultrasound-mediated drug release [23]. In the passive version, the release mechanisms of drugs contained into liposomes occurs by drug diffusion through the lipid bilayer and/or slow degradation of the lipid bilayer itself. The formulations for US-mediated release constitute a more flexible therapeutic approach, for example by formulating liposomes with temperature-sensitive phospholipid bilayers [24, 25] that can be disrupted upon US-induced mild hyperthermia ($40\text{--}42^\circ\text{C}$) to release the loaded drug.

Ultrasound-triggered drug-loaded microbubbles have the great potential in locally drug release and enhanced delivery to the target tissue. Roovers et al. showed that upon applying ultrasound, nanoparticle-loaded microbubbles can deposit nanoparticles onto cells, entitled sonoprinting [26]. They revealed that sonoprinting can also occur in more complex tissues, like monospheroids and cospheroids, resulting in a significant reduction in cell viability. Hence, some studies have proposed the use of permanent implanted magnets instead of external magnetic field application in the target organ. Pacheo et al. implemented a more promising and effective technique to attract the carbon-coated iron nanoparticles exposed to an implanted magnetic field [27, 28]. This technique leads to the release of drug at the tumor region more efficiently than application of external magnetic field. Escribano et al. investigated the in-vivo bio-distribution of carbon-coated iron nanoparticles in mice bearing an inflammatory focus exposed to magnetic field induced by a magnetic implant [29]. They indicated that mice with inflammatory regions are good alternatives in nanoparticle screening. Furthermore, they showed that selective bio-distribution in the target organ was increased when a low dose of nanoparticles was used.

Concerning the computational developments of this kind of applications to generate ultrasound from a magnetic field, Finite Element Method (FEM) simulations have been traditionally used to determine the magnetostatic interparticle forces and yield stress of the concentrated magneto-rheological fluids. In this procedure, the deformation of the particle lattice is measured in terms of elongation and rotation. This approach allows to solve the magnetostatic problem into an axisymmetric condition, which will result in lower computational costs in magnetic nanoparticle simulations [30, 31].

But the authors have not found any literature reference where magneto-mechanical multiphysics coupling for nanoparticle system is simulated. For this reasons, and according to the previous motivation in the present study, a multiphysics coupling model of magnetic nanoparticles behavior was performed. The main long term objective is to monitor the induced displacement signals and ultrasound generation

exposed to an alternating magnetic field. This novel model will enable to solve the problems in magnetic nanoparticle hyperthermia considering the interaction between solid mechanics compliance parameters and piezomagnetic coupling matrices. So, the first target presented in this paper is to generate a model and implement it computationally, assuring certain coherent behavior through some tests like a sensitivity analysis of the response to the variation of the model parameters.

This paper consists of a theoretical first part to present the multiphysics models, a second part describing the computational implementation to a particular case subject to be used in experiments and proposing a sensitivity analysis of the model parameters. Following, the results are described to end with a section with discussion and conclusions.

2. Theory

Magnetostriction describes the variation in dimensions of a material due to a change in its magnetization [32, 33]. The multiphysics constitutive equations are described in this section in the mechanical and magnetic field stress form. Hence, it would be necessary to implement the piezomagnetic properties of magnetic nanoparticles to solve the equations in magnetic hyperthermia.

2.1. Linear multiphysics model

The magnetostriction has a nonlinear dependence on the magnetic field and the mechanical stress in the material. However, the effect can be modeled using linear coupled constitutive equations if the response of the material consists of small deviations around an operating point. It is possible to express the relation between the stress S tensor, infinitesimal strain tensor ε , magnetic field vector H , and magnetic flux density vector B in either [34, 35] a stress-magnetization form,

$$\begin{cases} S = C_H \cdot \varepsilon - e_{HS}^T \cdot H \\ B = e_{HS} \cdot \varepsilon + \mu_0 \cdot \mu_{rs} \cdot H \end{cases} \quad (2)$$

or strain-magnetization form,

$$\begin{cases} \varepsilon = S_H \cdot S + d_{HT}^T \cdot H \\ B = d_{HT} \cdot S + \mu_0 \cdot \mu_{rT} \cdot H \end{cases} \quad (3)$$

where S is the stress [Pa], ε is the strain (adimensional), B is the magnetic flux density [T] (Tesla), H is the magnetic field [A/m] (A, ampere), C_H and S_H are the stiffness and compliance matrices measured at constant magnetic field, respectively ([Pa], [$1/Pa$]). The e_{HS} and d_{HT} are the piezo-magnetic coupling matrices ([T], [m/A]), μ_0 is the magnetic permeability of free space [N/A^2] (N, newton), μ_{rs} and μ_{rT} are the relative magnetic permeability measured at constant strain and stress (adimensional), respectively.

A partially nonlinear variant of the model can be explored, only considering the constitutive mechanical nonlinearity. This means to exchange the mechanical linear part of the equations $C_H \cdot \varepsilon$ (or $S_H \cdot S$) by a nonlinear stress-

strain relation. In the nonlinear case, the infinitesimal strain tensor ε is substituted in the constitutive equation by the Green-Lagrange finite strain tensor E and the stress tensor will be the second Piola-Kirchhoff stress tensor. In this research, as there is an interest in incompressible hyperelastic materials (presented later), special focus will be done in Mooney-Rivlin materials, applying the following three-parameter generalized Rivlin model [36–38], which expressed in terms of mechanical deformation energy W is,

$$W = A_{10}(I_{1C} - 3) + A_{01}(I_{2C} - 3) + A_{11}(I_{1C} - 3)(I_{2C} - 3) \quad (4)$$

where A_{10} and A_{01} are the mechanical parameters of the linear terms and A_{11} of the nonlinear term. I_{1C} and I_{2C} are the first and second principal invariants of the right Cauchy-Green deformation tensor C [39], being the third invariant $I_{3C} = 1$ for these incompressible materials.

The Green-Lagrange strain tensor E is related to the right Cauchy-Green tensor C through the simple relation $C = 2E + I$. Consequently, the first and second principal invariants I_1 and I_2 of E are $I_{1C} = 2I_1 + 3$ and $I_{2C} = 2I_2 + 3$ [39]. So, the energy in terms of the tensor E remains,

$$W = 2A_{10}I_1 + 2A_{01}I_2 + 4A_{11}I_1I_2 \quad (5)$$

The derivative of the energy W respect E results in the second Piola-Kirchhoff stress tensor S [40],

$$S = \frac{1}{2} \frac{\partial W}{\partial E} = A_{10}I + A_{01}I_1I - A_{01}E + 2A_{11}I_1^2I - 2A_{11}I_1E \quad (6)$$

with I the unity tensor, $\frac{\partial I_1}{\partial E} = I$ and $\frac{\partial I_2}{\partial E} = I_1I - E$ [40]. The right part of this expression should be inserted in the constitutive relation instead of the term $C_H \cdot \varepsilon$.

2.2. Finite element formulation

The governing discretized equation of motion of the system is written in the form (Eqs. 7 and 8).

$$M \cdot \partial_t^2 U + K \cdot U = F(t) \quad (7)$$

$$U^a = \begin{pmatrix} U_1^a \\ U_2^a \\ U_3^a \\ \phi^a \end{pmatrix} \quad (8)$$

where U and $\partial_t^2 U$ are the displacement and acceleration vectors including the three components of the displacements U_i^a and the magnetic degree of freedom ϕ^a , both associated to a node a of the spatial mesh, respectively, M is the mass matrix, K is the stiffness matrix and $F(t)$ is the time history of the applied load [41, 42].

The global stiffness matrix of the element can be expressed as (Eq. 9):

$$K = \int_V C^{(e)T} \cdot D \cdot C^{(e)} \cdot dV \quad (9)$$

where D is the elasticity matrix that transforms effective strains to stresses including the magnetic field coupling at every point of the domain. The strain magnetization-

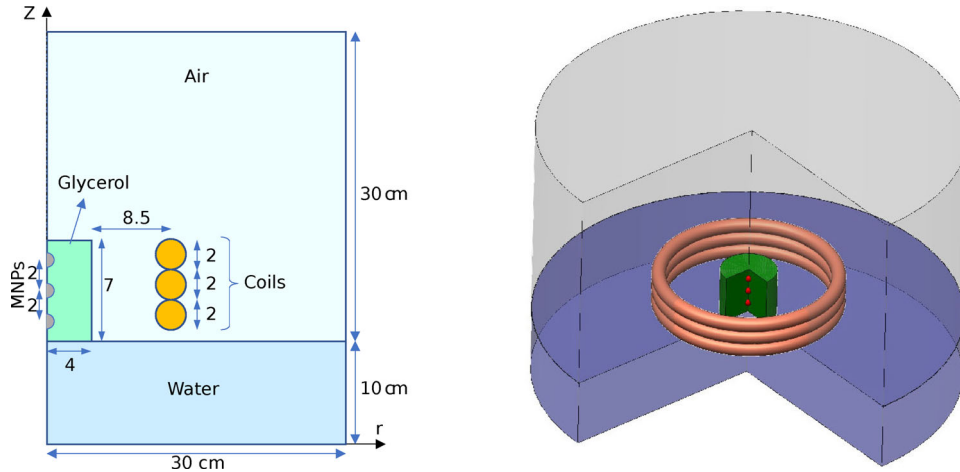


Figure 1. (left) 2D geometrical sketch of the indicating materials and dicase containing air, water, a three-turn coil, a glycerol container and three (magnified) magnetic nanoparticles located in the center and corners of the glycerol axis (right) 3D model by axymmetric revolution of the 2D case.

magnetostriction model implemented in this study is as described below (Eq. 10) [41].

magnetic field is created with a coil inside a cylindrical glycerol mass in which three ferromagnetic nanoparticles are

$$\begin{pmatrix} \varepsilon_{11} \\ \varepsilon_{22} \\ \varepsilon_{33} \\ \varepsilon_{12} \\ \varepsilon_{13} \\ \varepsilon_{23} \\ B_1 \\ B_2 \\ B_3 \end{pmatrix} = \begin{pmatrix} S_{H11} & S_{H12} & S_{H13} & 0 & 0 \\ S_{H12} & S_{H11} & S_{H13} & 0 & 0 \\ S_{H13} & S_{H13} & S_{H33} & 0 & 0 \\ 0 & 0 & 1 & S_{H44} & 0 \\ 0 & 0 & 1 & 0 & S_{H44} \\ 0 & 0 & 1 & 0 & 0 \\ 0 & 0 & 0 & 0 & d_{15} \\ 0 & 0 & 0 & d_{15} & 0 \\ d_{31} & d_{31} & d_{33} & 0 & 0 \end{pmatrix} \begin{pmatrix} 0 \\ 0 \\ 0 \\ 0 \\ 0 \\ 2(S_{H11} - S_{H12}) \\ 0 \\ 0 \\ 0 \end{pmatrix} + \begin{pmatrix} 0 & 0 & 0 & d_{31} \\ 0 & 0 & 0 & d_{31} \\ 0 & 0 & 0 & d_{33} \\ 0 & 0 & d_{15} & 0 \\ 0 & d_{15} & 0 & 0 \\ 0 & \mu_0 \mu_{11} & 0 & 0 \\ 0 & 0 & \mu_0 \mu_{11} & 0 \\ 0 & 0 & 0 & \mu_0 \mu_{11} \end{pmatrix} \begin{pmatrix} S_{11} \\ S_{22} \\ S_{33} \\ S_{12} \\ S_{13} \\ S_{23} \\ H_1 \\ H_2 \\ H_3 \end{pmatrix} \quad (10)$$

$$C^{(e)} = \begin{pmatrix} N_{,1}^a & 0 & 0 & 0 \\ 0 & N_{,2}^a & 0 & 0 \\ 0 & 0 & N_{,3}^a & 0 \\ N_{,2}^a & N_{,1}^a & 0 & 0 \\ N_{,3}^a & 0 & N_{,1}^a & 0 \\ 0 & N_{,3}^a & N_{,2}^a & 0 \\ 0 & 0 & 0 & N_{,1}^a \\ 0 & 0 & 0 & N_{,2}^a \\ 0 & 0 & 0 & N_{,3}^a \end{pmatrix} \quad (11)$$

where $C^{(e)}$ is the strain-displacement matrix of the element (e) of the spatial mesh, and the superscript T denotes the transpose operator, being $N_{,i}^a$, $i = 1, 2, 3$ the shape functions defined for each type of element (Eq. 11).

3. Case study and computational implementation

The computational implementation has been performed considering an experiment that will follow this study. A

embedded and distributed in its central axis. The numerical tool selected for solving the response of the model is the Finite Element Method (FEM) by using COMSOL Multiphysics 5.6. Given the radial symmetry, the 3-D simulation will be obtained by revolution of the 2-D results of the computation. Therefore, a plane mesh formed by 3-node triangular finite elements was chosen, with 4 degrees of freedom per node, as it is described in Eq. (11).

3.1. Geometry design

Figure 1 (left) show the radial section of the setup (rZ plane, a domain of 30×40 cm) where it can be observed a water base (30×10 cm base x height), on which it is resting half section of the glycerol cylinder (4×7 cm) being the cylinder's axis on the Z axis, both located at the left limit of the domain. Surrounding the glycerol and water mass there is air (30×30 cm). A three-turn circular coil, considered as a solenoid, is $\varnothing 25$ cm with a $\varnothing 2$ cm conductor's section. The symmetry axes of the coil, of the glycerol cylinder and Z are coinciding in space and located in the left margin of the domain. Finally, three semi-circular ferromagnetic nanoparticles

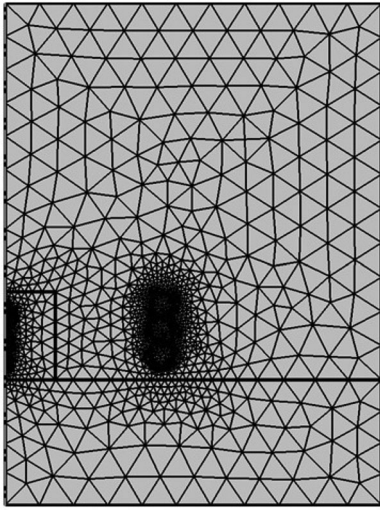


Figure 2. 2D meshed domain with triangular elements at different sizes.

(\odot 100 nm, magnified in size to allow observation in the figure) are separated 2 cm one each other and located on the axis of the glycerol container. The particle in the middle is at the center of the container height. The figure presents all the geometrical distances in centimeters. The size of the nanoparticles is magnified in the figure. The nanoparticles get a spherical shape by completing the rotation of the section rZ around Z to get the 3-D case (see Figure 1 right).

The boundary conditions are selected as the simplest case that implies that the magnetic flux density is null all over the boundary. The lack of vertical symmetry between the coil and the boundary will help to confirm that the computation is correct by observing the asymmetry of the results.

3.2. Mesh definition

The 2D model was meshed with triangular elements (Figure 2). Considering a normal mesh size, around 8342 domain elements and 630 boundary elements were created. It can be observed the smaller element size around the coils and the nanoparticles. The mesh is automatically created by COMSOL software which considers the dimensions of the elements in the domain.

3.3. Material properties

In the current research, the magnetostrictive linear model was considered in strain magnetization constitutive form for the magnetic nanoparticles. The material properties of nanoparticles were assumed the same as Magnetite but with Cobalt Ferrite ($CoFe_2O_4$) piezomagnetic properties, which exhibits the largest magnetostriction, embedded in a glycerol domain [43]. The compliance matrix was considered for description of the elasticity of the nanoparticles, while the piezomagnetic coupling matrices were introduced to simulate the magnetostrictive behavior of nanoparticles [44] (Table 1).

Table 1. Material properties introduced to the magnetite nanoparticles with cobalt ferrite piezomagnetic properties [45].

Material properties	Magnitude
Compliance coefficient S_{11} [1/GPa]	1/286
Compliance coefficient S_{12} [1/GPa]	1/173
Compliance coefficient S_{13} [1/GPa]	1/170
Compliance coefficient S_{33} [1/GPa]	1/269.5
Compliance coefficient S_{44} [1/GPa]	1/45.3
Piezo-magnetic coefficient d_{15} [m/A]	550
Piezo-magnetic coefficient d_{31} [m/A]	580.3
Piezo-magnetic coefficient d_{33} [m/A]	699.7
Relative permeability μ_{11}	2.5
Relative permittivity ϵ	8
Electrical conductivity σ [S/m]	10^{-3}

Table 2. Sampling ranges and intervals of the model and material parameters for the sensitivity study of the particle's displacement. The mesh size directly shows the 3 tested values.

Parameters	Range	Interval	Samples
Elastic modulus of MNPs [GPa]	[150, 250]	10	11
Radius of MNPs [nm]	[50, 200]	10	16
Distance between MNPs [mm]	[0, 6]	1	7
Elastic modulus of glycerol [kPa]	[1, 151]	10	16
Viscosity of glycerol [Pa · s]	[1, 5]	1	5
Maximum mesh element size [mm]	2.12, 2.68, 4		3

3.4. Excitation and time discretization

It has been shown that in an alternating magnetic field of frequency f , due to the alternating gradient, magnetic nanoparticles oscillate mechanically and generate ultrasound waves. Hence, in this study a sinusoidal function with a current amplitude intensity of 200 Amperes at the frequency of $f = 10^5$ Hz ($T = 10 \mu s$) was applied (Eq. 12).

$$I = 200 \cdot \sin(2\pi \cdot 10^5 \cdot t) \quad (12)$$

A sampling frequency $f_s = 200kHz$, twice the frequency of the excitation, would match the minimum Nyquist criterion. But in order to capture some nonlinear effects of 2nd or even 3rd harmonics, a sampling frequency of $f_s = 10 f = 1MHz$ is chosen, considering that 5th harmonics effects will be included. The time domain is established as 500 cycles of the excitation frequency, yielding 5 ms.

3.5. Sensitivity analysis

A range of independent model and material parameters were changed to see how the displacement results are consequently affected. The main parameters that were investigated are shown in Table 2 indicating the range of variation of the parameter ([first, last] values), the sampling interval, and the number of samples in the range.

4. Results

The results will be presented in the following way: first, some basic and trivial results to check that everything works as expected; checking that the distributions of magnetic flux density, stress and displacements present no evident strange behavior, as well as the confirmation of displacements in the magnetic nanoparticles. As a second part, the results of the sensibility analysis will be presented. These two previous

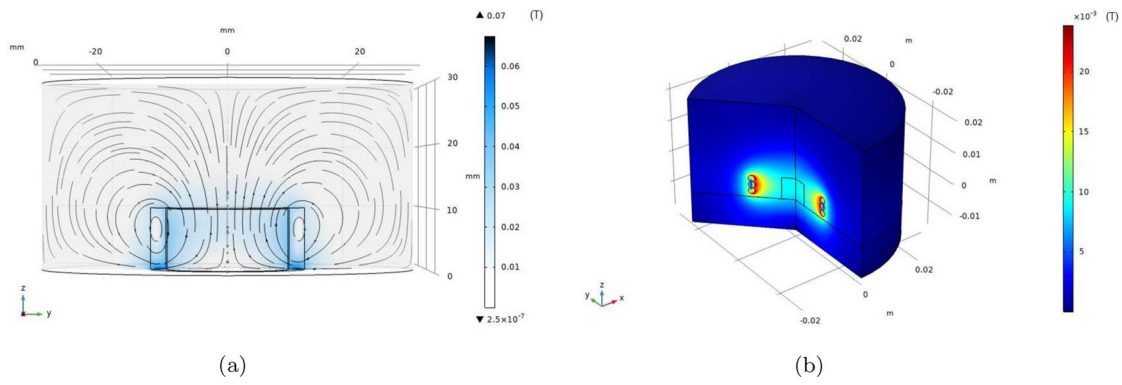


Figure 3. Computations of the magnetic flux density distribution. (a) A coil in air. Amplitude and field lines. (b) Case of study. Maximum amplitude distribution.

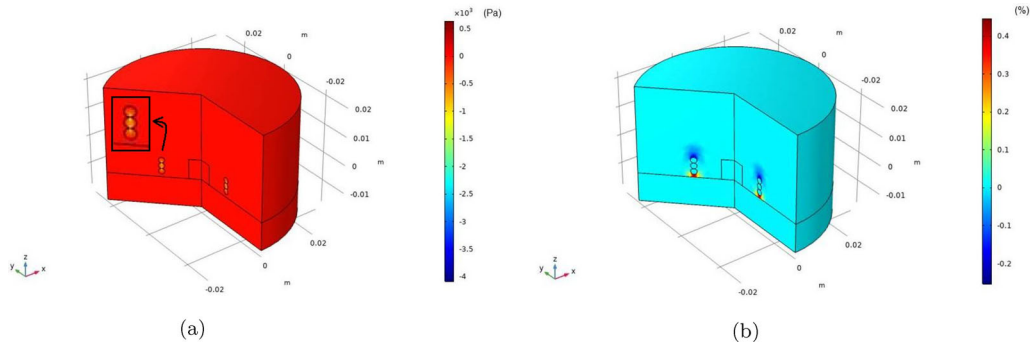


Figure 4. Mechanical effect of the coupling. (a) Z-Stress distribution σ_{zz} (Pa). (b) Z-Strain distribution ϵ_{zz} .

parts are performed with the linear model, so that in a last third part the computations with the mechanical nonlinear model are described.

Innitially, the computation of the magnetic flux distribution has been tested on a very simple case; only a coil in air without glycerol, nanoparticles, and the water eliminated from the domain so that the coil is supported on the lower boundary. Figure 3(a) shows the vertical asymmetry of the magnetic flux distribution due to asymmetric position of the coil related to the boundary. No anomalies are apparent in the results.

Figure 3(b) shows the results of the 3D revolved model of the case under study with the three assumed nanoparticles, located on the top, center and bottom of the glycerol container. The magnetic flux density was induced in the whole domain with the peak of the magnetic flux density is around coil and in lower magnitude in the space inside. Initially, the magnetic flux density seems to be correctly computed. The next step is to check that the induced magnetic flux density is able to generate mechanical stress, so that the magneto-mechanical coupling is computed. Figure 4(a) shows the vertical component of the stress σ_{zz} , where the higher absolute values appear around the coils in slight yellow color. Significant deformation is also observed in the area of the coils in Figure 4(b), higher at the bottom coil and lower at the upper one. This is due to the higher gradient of the magnetic induction at the bottom. This information of the figures means that a magneto-mechanical coupling is being computed and the results seem to be coherent. Concerning the mechanical effects at the magnetic

nanoparticles, their stresses and strains cannot be observed in the previous figures, because its lower order of magnitude in amplitude compared to the points around the coils. But the results indicate that the three nanoparticles underwent displacements of a magnitude in the order of 10^{-12} m (Figure 5a). The output signal showed different displacement trends in Z-axis, but within the same order of magnitude for the three nanoparticles. The initial time of the Z component of the displacement, equivalent to two excitation periods ($20\mu\text{s}$) is showed in Figure 5(b). The particles present a component of oscillation around the excitation frequency that is superimposed on the previous one and is several orders of magnitude lower. Additional tests have been made, where (a) the magnetic features of the three nanoparticles has been removed, leading to null displacements, and (b) only the magnetic features of the center particle are maintained, resulting in a displacement shown in Figure 6, a different signal than that with 3 magnetic nanoparticles. This means that the presence of the the top and bottom nanoparticles modify the displacement of the center particle.

The results of the sensitivity analysis revealed the fact that the magnitude of the displacements induced is not dependent to the elastic modulus of the magnetic nanoparticles, viscosity of glycerol medium and the mesh element size. The distance between the two magnetic nanoparticles was found to have an effect on the magnitude of the displacements. The highest Maximum magnitude of Z-axis displacement was found when the two nanoparticles were 5 mm away from each other, in a 7 mm glycerol container (Table 3). The size of the nanoparticles were also found to

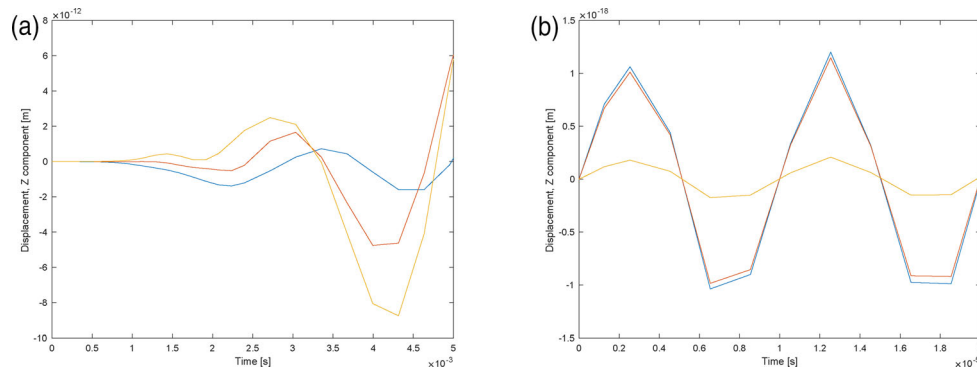


Figure 5. (a) Component Z of the displacement of the three nanoparticles: orange line = bottom, red line = middle and blue line = top (b) First two cycles of the displacements in Z of the three nanoparticles: orange line = bottom, red line = middle and blue line = top.

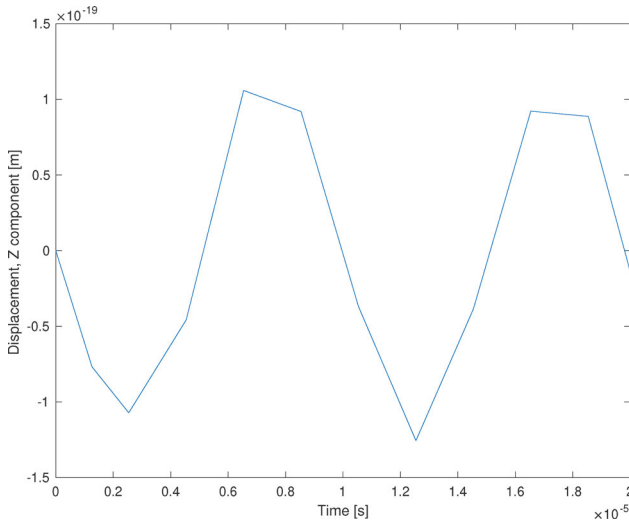


Figure 6. The Z-component of the displacement of the magnetic nanoparticle in the center, removing the magnetic features of the top and bottom nanoparticles.

have an effect on the induced displacement signals of magnetic nanoparticles, within the range of 50-200 nm (Figure 7).

A wide range of elasticity and viscosity parameters were chosen for the glycerol, which enabled us to monitor the sensitivity of the displacement signals of magnetic nanoparticles to the viscoelasticity of the medium. The amplitude and frequency of the displacement signals were affected by the change in the elastic properties of the glycerol, not to the viscosity (Figure 8).

The generalized Mooney-Rivlin hyperelastic models were introduced to the glycerol medium and the displacement signals of magnetic nanoparticles were extracted. The three Mooney-Rivlin models were chosen based on the three different gel concentrations at different modes of deformation [36]. The results showed that magnetic nanoparticle displacement signals are not dependent to different Mooney-Rivlin model coefficients at different modes of deformation and gel concentrations of glycerol medium (Table 4).

5. Discussion & conclusion

In the present study, a multiphysics coupling model of magnetic nanoparticle behavior was developed, implementing

Table 3. Sensitivity analysis of the displacement results to the distance between the two magnetic nanoparticles at 500 cycles of excitation in Z-direction.

Distance between two MNPs [m]	Maximum magnitude of displacement [m]
$h = 0$	$1.788 \cdot 10^{-11}$
$h = 1 \cdot 10^{-3}$	$1.788 \cdot 10^{-11}$
$h = 2 \cdot 10^{-3}$	$1.788 \cdot 10^{-11}$
$h = 3 \cdot 10^{-3}$	$1.787 \cdot 10^{-11}$
$h = 4 \cdot 10^{-3}$	$1.734 \cdot 10^{-11}$
$h = 5 \cdot 10^{-3}$	$1.828 \cdot 10^{-11}$
$h = 6 \cdot 10^{-3}$	$1.787 \cdot 10^{-11}$

solid mechanics compliance matrix and piezomagnetic coupling matrices. The oscillation of the nanoparticles is due to the alternating magnetic field. The results revealed that the assumed nanoparticles at different locations may have similar behavior at the same order of magnitude of displacements. The results of the displacement graph along the vertical Z-axis, showed that the nanoparticles drift upward after some initial oscillations. The assumed nanoparticle at the bottom of the glycerol container underwent oscillations with the highest amplitude induced by a magnetic force repelling it from the locations. This phenomenon could be due to the maximum magnetic flux gradient in the domain as the magnetic flux density arrays converge on the bottom and diverge on top of the container. The displacement graphs in Z-direction did not show any significant changes in the behavior and magnitude of displacements for the assumed nanoparticles.

Moreover, the model was modified by comparing the displacement signals for the two cases; with one central MNP and the other with three MNPs on the top, bottom and in the center of the glycerol medium. The results modified the fact that the magnitude of displacements would increase by increasing the number of the nanoparticles, while the signal behavior didn't differ for the two models. This change could be attributed to the magnetization effect, as a result of piezomagnetic properties, which can induce higher stress by increasing the number of the magnetic nanoparticles.

The results of the sensitivity analysis indicated that the displacement signals may be affected by some geometric or material parameters in the model. The distance between the two magnetic nanoparticles changed some characteristics of the displacement signals. This effect was found to result in

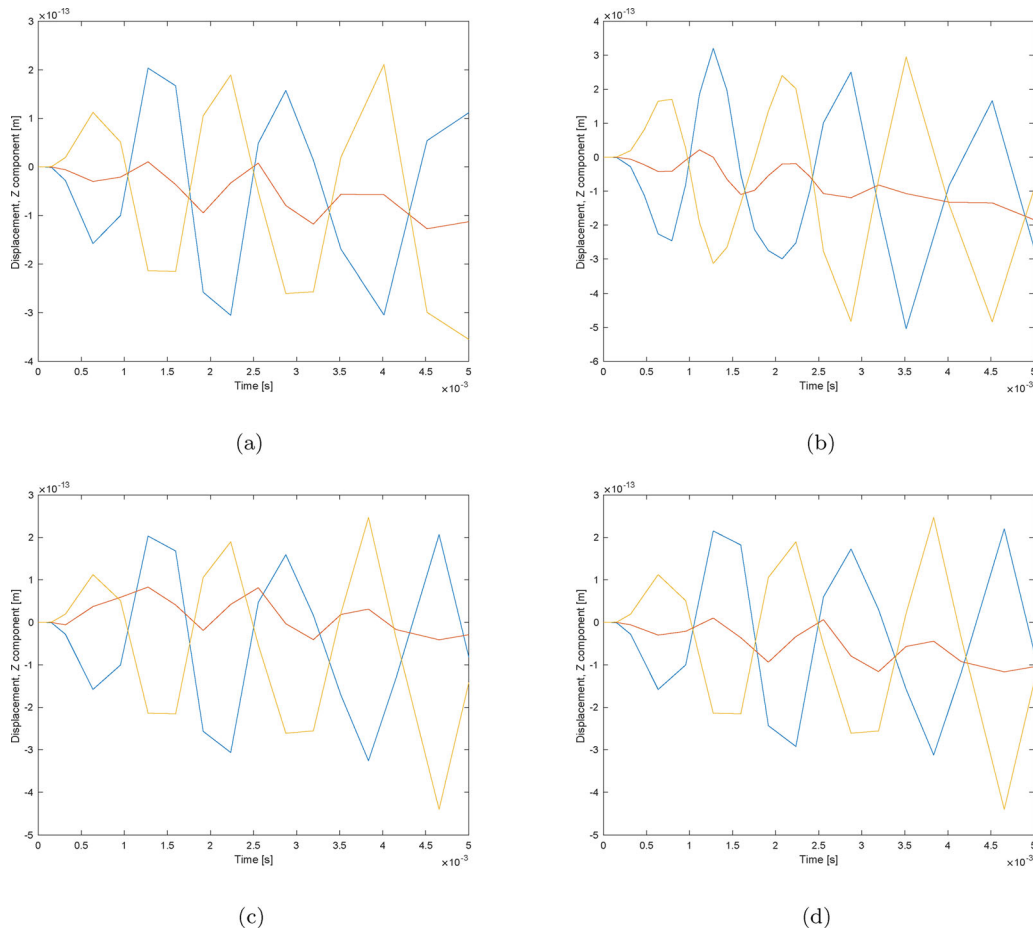


Figure 7. The Z-component displacement of the three nanoparticles varying their size (radius); orange = bottom, red = middle and blue = top. (a) Particle radii $R = 50$ nm. (b) $R = 100$ nm. (c) $R = 150$ nm. (d) $R = 200$ nm.

Table 4. The generalized Mooney-Rivlin hyperelastic model coefficients introduced to the glycerol medium [36].

Mode of deformation	Gel concentration [%w/v]	A_{10} [KPa]	A_{01} [KPa]	A_{11} [KPa]
Compression	1.5	-67.67	81.81	-32.44
	2.5	21.01	23.69	-15.15
	4	-252.72	320.94	-120.03
Tension	1.5	17.17	15.28	343.74
	2.5	-51.52	122.86	609.71
	4	-176.02	327.73	744.29
Comp.+Tension	1.5	93.88	-66.26	35.89
	2.5	246.90	-184.83	89.22
	4	430.61	-307.44	180.44
Comp.+Tension + Shear	1.5	83.14	-56.43	31.39
	2.5	203.47	-145.26	71.26
	4	415.17	-293.74	175.62

the maximum displacement when the two magnetic nanoparticles were located 5 millimeters away one another, one on the top and the other on the bottom of the glycerol container. This distance seems to be far enough for the maximum magnetization effect between the two magnetic nanoparticles. The magnetization effect can also be related to the induced wave length of the magnetic nanoparticle displacement signals. In addition, the size of the magnetic nanoparticle was found to change the amplitude of the displacement signals, which had been proved theoretically (Eq. 1) [8]. Hence, an increase in the radius of magnetic nanoparticles resulted in an increase in the amplitude of the displacement signals, while the elastic modulus of the

nanoparticles and the mesh element size did not show any effect on the displacement signals.

Moreover, the elastic properties of the glycerol medium found to have an effect on the amplitude and frequency of the nanoparticle displacement signals. The results revealed that by increasing the elasticity of the glycerol, the frequency of the nanoparticle displacement signals increased, while a decrease in the amplitude was observed. Consequently, the magnetic nanoparticles were found to undergo displacements at a wide range of frequency from 100 Hz to 600 Hz for different elastic modulus of glycerol from 3 KPa to 150 KPa. Unlikely, The viscosity of the glycerol didn't change any parameter in the displacement signals of the magnetic

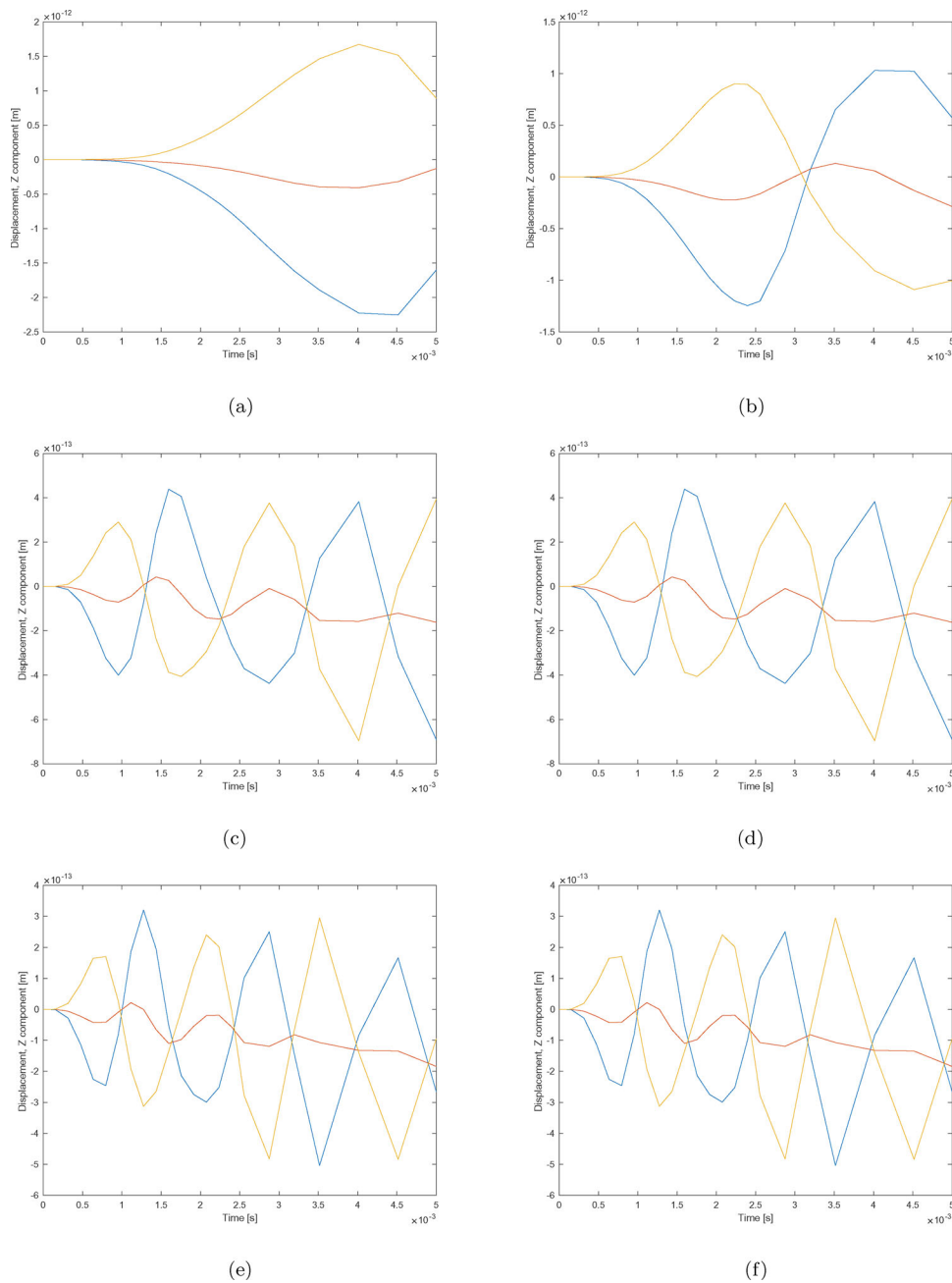


Figure 8. Component Z of displacement of the nanoparticles in the glycerol medium varying the elasticity and viscosity coefficients; orange line = bottom, red line = middle and blue line = top. (a) $E = 3 \text{ KPa}$, $\eta = 0 \text{ Pa.s}$. (b) $E = 10 \text{ KPa}$, $\eta = 0 \text{ Pa.s}$. (c) $E = 75 \text{ KPa}$, $\eta = 0 \text{ Pa.s}$. (d) $E = 75 \text{ KPa}$, $\eta = 5 \text{ Pa.s}$. (e) $E = 150 \text{ KPa}$, $\eta = 0 \text{ Pa.s}$. (f) $E = 150 \text{ KPa}$, $\eta = 5 \text{ Pa.s}$.

nanoparticles. Similarly, The results showed that magnetic nanoparticle displacement signals are not dependent on different Mooney-Rivlin model coefficients at different modes of deformation and gel concentrations of glycerol medium.

The results revealed that the magnetic nanoparticles undergo some displacements when they are exposed to an alternating magnetic field. These oscillations can lead to ultrasound generation [8], though, the amplitude of displacement signal for each nanoparticle is negligibly small. It is expected that aggregated nanoparticles result in much higher oscillations which can be very useful for an efficient targeting in drug delivery. It could also permit for ultrasound therapy at the cell level, in cells which have internalized magnetic nanoparticles.

The main limitation of this study was the difficulty in the accurate modeling of the number of magnetic nanoparticles within the hydrogel medium, compared to the experimental setup, which constrained the results for direct clinical applications. Moreover, for the revolution, only nanoparticles were constrained at definite locations along the vertical Z-axis. This assumption was a simplicity to model the random distribution of nanoparticles within the medium.

In conclusion, an optimized modellization of three magnetic nanoparticles exposed to an alternating magnetic field may result in ultrasound generation in 3D. This phenomenon may lead to a more efficient targeting in drug delivery or inducing a change in pathological cells without increase in the temperature.

Acknowledgment

The authors would like to thank Nanoscience Institute of Zaragoza for their support running the models and motivating the conceptualization of this research.

Conflict of interests

The authors declare no conflict of interests.

Funding

This research was funded by the Ministry of Science and Innovation, Spain grant numbers PID2019-106947RA-C22 and (FEDER) EQC2018-004508-P.

ORCID

A. Ashofteh  <http://orcid.org/0000-0003-1343-576X>
 R. Marqués  <http://orcid.org/0000-0002-3328-720X>
 A. Callejas  <http://orcid.org/0000-0002-8506-5166>
 R. Muñoz  <http://orcid.org/0000-0002-4137-7184>
 J. Melchor  <http://orcid.org/0000-0002-5542-1588>

References

- [1] L. Asin, G.F. Goya, A. Tres, and M.R. Ibarra, Induced cell toxicity originates dendritic cell death following magnetic hyperthermia treatment, *Cell Death Dis.*, vol. 4, no. 4, pp. e596–e596, 2013. DOI: [10.1038/cddis.2013.121](https://doi.org/10.1038/cddis.2013.121).
- [2] L. Asin, M.R. Ibarra, A. Tres, and G.F. Goya, Controlled cell death by magnetic hyperthermia: effects of exposure time, field amplitude, and nanoparticle concentration, *Pharm Res.*, vol. 29, no. 5, pp. 1319–1327, 2012.
- [3] B. Sanz, M.P. Calatayud, T.E. Torres, M.L. Fanarraga, M.R. Ibarra, and G.F. Goya, Magnetic hyperthermia enhances cell toxicity with respect to exogenous heating, *Biomaterials.*, vol. 114, pp. 62–70, 2017. DOI: [10.1016/j.biomaterials.2016.11.008](https://doi.org/10.1016/j.biomaterials.2016.11.008).
- [4] F. Gazeau, M. Lévy, and C. Wilhelm, Optimizing magnetic nanoparticle design for nanothermotherapy, 2008.
- [5] P. Guardia, R. Di Corato, L. Lartigue, C. Wilhelm, A. Espinosa, M. Garcia-Hernandez, F. Gazeau, L. Manna, and T. Pellegrino, Water-soluble iron oxide nanocubes with high values of specific absorption rate for cancer cell hyperthermia treatment, *ACS Nano.*, vol. 6, no. 4, pp. 3080–3091, 2012. DOI: [10.1021/nn2048137](https://doi.org/10.1021/nn2048137).
- [6] M. Creixell, A.C. Bohorquez, M. Torres-Lugo, and C. Rinaldi, EGFR-targeted magnetic nanoparticle heaters kill cancer cells without a perceptible temperature rise, *ACS Nano.*, vol. 5, no. 9, pp. 7124–7129, 2011. DOI: [10.1021/nn201822b](https://doi.org/10.1021/nn201822b).
- [7] A. Villanueva, P. de la Presa, J.M. Alonso, T. Rueda, A. Martínez, P. Crespo, M.P. Morales, M.A. Gonzalez-Fernandez, J. Valdés, and G. Rivero, Hyperthermia hela cell treatment with silica-coated manganese oxide nanoparticles, *J. Phys. Chem. C.*, vol. 114, no. 5, pp. 1976–1981, 2010. DOI: [10.1021/jp907046f](https://doi.org/10.1021/jp907046f).
- [8] J. Carrey, V. Connord, and M. Respaud, Ultrasound generation and high-frequency motion of magnetic nanoparticles in an alternating magnetic field: toward intracellular ultrasound therapy?, *Appl. Phys. Lett.*, vol. 102, no. 23, pp. 232404, 2013. DOI: [10.1063/1.4810972](https://doi.org/10.1063/1.4810972).
- [9] B. Thiesen, and A. Jordan, Clinical applications of magnetic nanoparticles for hyperthermia, *Int. J. Hyperth.*, vol. 24, no. 6, pp. 467–474, 2008. DOI: [10.1080/02656730802104757](https://doi.org/10.1080/02656730802104757).
- [10] M. Salloum, R. Ma, and L. Zhu, Enhancement in treatment planning for magnetic nanoparticle hyperthermia: optimization of the heat absorption pattern, *Int. J. Hyperth.*, vol. 25, no. 4, pp. 309–321, 2009.
- [11] A. Candeo, and F. Dughiero, Numerical fem models for the planning of magnetic induction hyperthermia treatments with nanoparticles, *IEEE Trans. Magn.*, vol. 45, no. 3, pp. 1658–1661, 2009. DOI: [10.1109/TMAG.2009.2012769](https://doi.org/10.1109/TMAG.2009.2012769).
- [12] Y. Tang, R.C.C. Flesch, and T. Jin, Numerical analysis of temperature field improvement with nanoparticles designed to achieve critical power dissipation in magnetic hyperthermia, *J. Appl. Phys.*, vol. 122, no. 3, pp. 034702, 2017. DOI: [10.1063/1.4994309](https://doi.org/10.1063/1.4994309).
- [13] M. Pavel, and A. Stancu, Ferromagnetic nanoparticles dose based on tumor size in magnetic fluid hyperthermia cancer therapy, *IEEE Trans. Magn.*, vol. 45, no. 11, pp. 5251–5254, 2009. DOI: [10.1109/TMAG.2009.2031076](https://doi.org/10.1109/TMAG.2009.2031076).
- [14] H.G. Bagaria, and D.T. Johnson, Transient solution to the bio-heat equation and optimization for magnetic fluid hyperthermia treatment, *Int. J. Hyperth.*, vol. 21, no. 1, pp. 57–75, 2005. DOI: [10.1080/02656730410001726956](https://doi.org/10.1080/02656730410001726956).
- [15] M. Lahonian, and A.A. Golneshan, Numerical study of temperature distribution in a spherical tissue in magnetic fluid hyperthermia using lattice Boltzmann method, *IEEE Trans. Nanobiosci.*, vol. 10, no. 4, pp. 262–268, 2011. DOI: [10.1109/TNB.2011.2177100](https://doi.org/10.1109/TNB.2011.2177100).
- [16] L. Wu, J. Cheng, W. Liu, and X. Chen, Numerical analysis of electromagnetically induced heating and bioheat transfer for magnetic fluid hyperthermia, *IEEE Trans. Magn.*, vol. 51, no. 2, pp. 1–4, 2015. DOI: [10.1109/TMAG.2014.2358268](https://doi.org/10.1109/TMAG.2014.2358268).
- [17] J. Li, H. Yao, Y. Lei, W. Huang, and Z. Wang, Numerical simulation of magnetic fluid hyperthermia based on multiphysics coupling and recommendation on preferable treatment conditions, *Curr. Appl. Phys.*, vol. 19, no. 9, pp. 1031–1039, 2019. DOI: [10.1016/j.cap.2019.06.003](https://doi.org/10.1016/j.cap.2019.06.003).
- [18] M. Salloum, R.H. Ma, D. Weeks, and L. Zhu, Controlling nanoparticle delivery in magnetic nanoparticle hyperthermia for cancer treatment: experimental study in agarose gel, *Int. J. Hyperth.*, vol. 24, no. 4, pp. 337–345, 2008.
- [19] W. Lin, Introduction: nanoparticles in medicine, 2015.
- [20] S. Tong, H. Zhu, and G. Bao, Magnetic iron oxide nanoparticles for disease detection and therapy, *Mater. Today (Kidlington)*, vol. 31, pp. 86–99, 2019. DOI: [10.1016/j.mattod.2019.06.003](https://doi.org/10.1016/j.mattod.2019.06.003).
- [21] M.D. Gray, P.C. Lyon, C. Mannaris, L.K. Folkes, M. Stratford, L. Campo, D.Y.F. Chung, S. Scott, M. Anderson, R. Goldin, R. Carlisle, F. Wu, M.R. Middleton, F.V. Gleeson, and C.C. Coussios, Focused ultrasound hyperthermia for targeted drug release from thermosensitive liposomes: results from a phase I trial, *Radiology.*, vol. 291, no. 1, pp. 232–238, 2019.
- [22] T.M. Allen, and P.R. Cullis, Drug delivery systems: entering the mainstream, *Science.*, vol. 303, no. 5665, pp. 1818–1822, 2004. DOI: [10.1126/science.1095833](https://doi.org/10.1126/science.1095833).
- [23] O. Couture, J. Foley, N.F. Kassell, B. Larrat, and J.-F. Aubry, Review of ultrasound mediated drug delivery for cancer treatment: updates from pre-clinical studies, *Transl. Cancer Res.*, vol. 3, no. 5, pp. 494–511, 2014.
- [24] M.B. Yatvin, J.N. Weinstein, W.H. Dennis, and R. Blumenthal, Design of liposomes for enhanced local release of drugs by hyperthermia, *Science*, vol. 202, no. 4374, pp. 1290–1293, 1978. DOI: [10.1126/science.364652](https://doi.org/10.1126/science.364652).
- [25] R. Chandan, and R. Banerjee, Pro-apoptotic liposomes-nanobubble conjugate synergistic with paclitaxel: a platform for ultrasound responsive image-guided drug delivery, *Sci Rep.*, vol. 8, no. 1, pp. 1–15, 2018. DOI: [10.1038/s41598-018-21084-8](https://doi.org/10.1038/s41598-018-21084-8).
- [26] S. Roovers, J. Deprez, D. Priwitaningrum, G. Lajoinie, N. Rivron, H. Declercq, O. De Wever, E. Stride, S. Le Gac, M. Versluis, J. Prakash, S.C. De Smedt, and I. Lentacker, Sonoprinting liposomes on tumor spheroids by microbubbles and ultrasound, *J. Control Release.*, vol. 316, pp. 79–92, 2019. DOI: [10.1016/j.jconrel.2019.10.051](https://doi.org/10.1016/j.jconrel.2019.10.051).
- [27] R. Fernández-Pacheco, C. Marquina, J. Gabriel Valdivia, M. Gutiérrez, M. Soledad Romero, R. Cornudella, A. Laborda, A. Viloria, T. Higuera, A. García, J. Antonio García de Jalón, and M. Ricardo Ibarra, Magnetic nanoparticles for local drug delivery

- using magnetic implants, *J. Magn. Magn. Mater.*, vol. 311, no. 1, pp. 318–322, 2007. DOI: [10.1016/j.jmmm.2006.11.192](https://doi.org/10.1016/j.jmmm.2006.11.192).
- [28] R. Fernández-Pacheco, J.G. Valdivia, and M.R. Ibarra. Magnetic nanoparticles for local drug delivery using magnetic implants, in *Micro and Nano Technologies in Bioanalysis*. Springer, Humana Press, Totowa, NJ, 2009. pp. 559–569.
- [29] E. Escribano, R. Fernández-Pacheco, J.G. Valdivia, M.R. Ibarra, C. Marquina, and J. Queralt, Effect of magnet implant on iron biodistribution of Fe_3O_4 nanoparticles in the mouse, *Arch. Pharm. Res.*, vol. 35, no. 1, pp. 93–100, 2012. DOI: [10.1007/s12272-012-0109-8](https://doi.org/10.1007/s12272-012-0109-8).
- [30] J.R. Morillas, and J. de Vicente, Dem and fem simulations in magnetorheology: aggregation kinetics and yield stress, *Magnetorheol. Mater. Appl.*, vol. 58, pp. 19, 2019.
- [31] Jose.R. Morillas, and Juan de Vicente, On the importance of interchain interaction and rotational contribution to the computation of the yield stress in magnetorheology, *Smart Mater. Struct.*, vol. 28, no. 8, pp. 08LT01, 2019. DOI: [10.1088/1361-665X/ab2470](https://doi.org/10.1088/1361-665X/ab2470).
- [32] S. Chikazumi, S. Chikazumi, and C.D. Graham, *Physics of Ferromagnetism*. Number 94. Oxford University Press, 1997.
- [33] H. Kronmüller, General micromagnetic theory, in *Handbook of Magnetism and Advanced Magnetic Materials*, John Wiley & Sons, 2007.
- [34] X. Liu, and X. Zheng, A nonlinear constitutive model for magnetostrictive materials, *Acta Mech Sinica.*, vol. 21, no. 3, pp. 278–285, 2005. DOI: [10.1007/s10409-005-0028-8](https://doi.org/10.1007/s10409-005-0028-8).
- [35] C.H. Sherman, and J.L. Butler, *Transducers and Arrays for Underwater Sound*, vol. 4. Springer, New York, 2007.
- [36] K. Upadhyay, G. Subhash, and D. Spearot, Hyperelastic constitutive modeling of hydrogels based on primary deformation modes and validation under 3d stress states, *Int. J. Eng. Sci.*, vol. 154, pp. 103314, 2020. DOI: [10.1016/j.ijengsci.2020.103314](https://doi.org/10.1016/j.ijengsci.2020.103314).
- [37] R.S. Rivlin, and G.I. Taylor, Large elastic deformations of isotropic materials. I. Fundamental concepts, *Philos. Trans. R. Soc. Lond. Ser. A, Math. Phys. Sci.*, vol. 240, no. 822, pp. 459–490, 1948.
- [38] R.S. Rivlin, and E.K. Rideal, Large elastic deformations of isotropic materials. IV. Further developments of the general theory, *Philos. Trans. R. Soc. Lond. Ser. A, Math. Phys. Sci.*, vol. 241, no. 835, pp. 379–397, 1948.
- [39] A.C. Eringen, and E.S. Suhubi, *Elastodynamics*, vol. I. New York, and London: Academic Press, 1974.
- [40] G.A. Holzapfel, *Nonlinear Solid Mechanics*, vol. 24. Chichester, UK: John Wiley & Sons, 2000.
- [41] J. Melchor, and G. Rus, Torsional ultrasonic transducer computational design optimization, *Ultrasonics.*, vol. 54, no. 7, pp. 1950–1962, 2014. DOI: [10.1016/j.ultras.2014.05.001](https://doi.org/10.1016/j.ultras.2014.05.001).
- [42] J. Melchor, R. Muñoz, and G. Rus, Torsional ultrasound sensor optimization for soft tissue characterization, *Sensors.*, vol. 17, no. 6, pp. 1402, 2017. DOI: [10.3390/s17061402](https://doi.org/10.3390/s17061402).
- [43] S. Srinivas, J.Y. Li, Y.C. Zhou, and A.K. Soh, The effective magnetoelastic moduli of matrix-based multiferroic composites, *J. Appl. Phys.*, vol. 99, no. 4, pp. 043905, 2006. DOI: [10.1063/1.2173035](https://doi.org/10.1063/1.2173035).
- [44] A.A. Yazdi, A.C. Zafra, P. Moreno, R. Muñoz, and J. Melchor, A numerical approach to the magnetic nanoparticle hyperthermia. In *2021 IEEE UFFC Latin America Ultrasonics Symposium (LAUS)*, pages 1–4. Oct., 2021.
- [45] J.H. Huang, and W.-s. Kuo, The analysis of piezoelectric/piezomagnetic composite materials containing ellipsoidal inclusions, *J. Appl. Phys.*, vol. 81, no. 3, pp. 1378–1386, 1997. DOI: [10.1063/1.363874](https://doi.org/10.1063/1.363874).